

Contents lists available at ScienceDirect

Bioactive Materials

journal homepage: www.keaipublishing.com/en/journals/bioactive-materials





Magnesium surface-activated 3D printed porous PEEK scaffolds for *in vivo* osseointegration by promoting angiogenesis and osteogenesis

Xinghui Wei ^{a,1}, Wenhao Zhou ^{b,1}, Zhen Tang ^{a,1}, Hao Wu ^a, Yichao Liu ^a, Hui Dong ^a, Ning Wang ^a, Hai Huang ^a, Shusen Bao ^a, Lei Shi ^c, Xiaokang Li ^{a,***}, Yufeng Zheng ^{d,e,**}, Zheng Guo ^{a,*}

- ^a Department of Orthopaedics, Tangdu Hospital, Fourth Military Medical University, Xi'an, Shaanxi, 710038, China
- b Northwest Institute for Nonferrous Metal Research, Xi'an, Shaanxi, 710016, China
- ^c Department of Orthopaedics, Xijing Hospital, Fourth Military Medical University, Xi'an, Shaanxi, 710032, China
- d Academy for Advanced Interdisciplinary Studies, Peking University, Beijing, 100871, China
- ^e Department of Materials Science and Engineering, College of Engineering, Peking University, Beijing, 100871, China

ARTICLE INFO

Keywords: Polyetheretherktone Porous Magnesium Angiogenesis Osteogenesis

ABSTRACT

Polyetheretherketone (PEEK) has been an alternative material for titanium in bone defect repair, but its clinical application is limited by its poor osseointegration. In this study, a porous structural design and activated surface modification were used to enhance the osseointegration capacity of PEEK materials. Porous PEEK scaffolds were manufactured via fused deposition modeling and a polydopamine (PDA) coating chelated with magnesium ions (Mg²⁺) was utilized on the surface. After surface modification, the hydrophilicity of PEEK scaffolds was significantly enhanced, and bioactive Mg²⁺ could be released. *In vitro* results showed that the activated surface could promote cell proliferation and adhesion and contribute to osteoblast differentiation and mineralization; the released Mg²⁺ promoted angiogenesis and might contribute to the formation of osteogenic H-type vessels. Furthermore, porous PEEK scaffolds were implanted in rabbit femoral condyles for *in vivo* evaluation of osseointegration. The results showed that the customized three-dimensional porous structure facilitated vascular ingrowth and bone ingrowth within the PEEK scaffolds. The PDA coating enhanced the interfacial osseointegration of porous PEEK scaffolds and the released Mg²⁺ accelerated early bone ingrowth by promoting early angiogenesis during the coating degradation process. This study provides an efficient solution for enhancing the osseointegration of PEEK materials, which has high potential for translational clinical applications.

1. Introduction

Bone grafting is the key surgical technique for repair and reconstruction of bone defects, and more than 2 million bone transplants are performed each year worldwide [1]. Due to the shortage of natural bone sources, ceramic, metal, polymer and other artificial bone graft materials are widely used in clinical applications [2–5]. Metallic materials such as tantalum, titanium and their alloys are mechanically strong and suitable for the repair of bone defects in load-bearing areas, making them the preferred support materials for large bone defects. However,

their high elastic modulus often causes stress shielding effects, which can lead to complications such as loosening of the prosthesis and bone resorption around the prosthesis during long-term implantation [3]. Polyetheretherketone (PEEK) materials are polymeric materials with stable physicochemical properties and high structural strength. The elastic modulus of PEEK materials is close to that of natural cancellous bone, and they are wear resistant, corrosion resistant, fatigue resistant, and biologically safe [6,7]. Thus, they are considered to be one of the most promising alternatives to titanium.

However, the surface of PEEK materials is hydrophobic and

Peer review under responsibility of KeAi Communications Co., Ltd.

^{*} Corresponding author. Department of Orthopaedics, Tangdu Hospital, Fourth Military Medical University, Xi'an, Shaanxi, 710038, China.

^{**} Corresponding author. Academy for Advanced Interdisciplinary Studies, Peking University, Beijing, 100871, China.

^{***} Corresponding author.

E-mail addresses: lxkfmmu@163.com (X. Li), yfzheng@pku.edu.cn (Y. Zheng), guozheng@fmmu.edu.cn (Z. Guo).

 $^{^{1}\,}$ These authors have contributed equally to this study.

biologically inert, resulting in poor osseointegration [8]. The introduction of 3-dimensional porous structures in PEEK materials can provide space for bone ingrowth, which will enhance the bone-implant bond strength [6,9]. Fused deposition modeling (FDM) is a 3-dimensional printing method for PEEK implants. Compared to traditional injection molding, it offers certain advantages such as simplified processes, improved timeliness, lower costs, and the ability to create a customized prosthesis to match the bone defect site [10,11]. Current studies have suggested that pore sizes larger than 100 μm can provide sufficient space for vascularization, nutrients supply, waste removal, and oxygen diffusion [12], and the recommended interconnected macropore structures of 300-500 µm are better for adequate capillary and bone ingrowth [13, 14]. Thus, customized porous structures are important for overcoming the inertness of PEEK materials and promoting osseointegration in vivo. Nonetheless, 3D printing technology does not change the bioactivity of the PEEK material, and further bioactive modifications is still needed.

Incorporating biodegradable bioactive materials, such as β -TCP, into PEEK materials is a promising approach to enhance the bioactivity of PEEK materials, but the introduction of new materials may reduce the mechanical stability of PEEK scaffolds [15]. Because of the complex shape, many surface modifications for solid PEEK materials are not applicable to porous PEEK due to the line-of-sight limitation [6]. Polydopamine (PDA) coating was easy to form a 50 nm thick coating inside the pores through simple dip-coating of objects in an aqueous solution of dopamine [16]. The PDA coating has excellent biocompatibility, and the abundant functional groups such as carboxyl, amino, and imino groups can serve as a "bridge" to further react with other compounds through secondary reactions [17]. Therefore, PDA not only forms a complete and dense activation layer on the porous PEEK surface but also completely transforms the surface properties (hydrophobicity, etc.) and provides adhesive basis for further activation.

To date, the bioactivity of modified PEEK materials is often achieved through the release of bioactive molecules or ions. Among them, magnesium ions are of great interest due to their rich biological functions. Mg²⁺ is the fourth most abundant cation in the body, and there are increasing evidences that Mg²⁺ can promote angiogenesis [18,19] and accelerate osteogenesis [20–22]. Incorporating magnesium into PEEK materials [23,24] or immobilizing magnesium on the surface of PEEK [25,26] have been important strategies to enhance the bioactivities of PEEK material. Considering that the mechanical strength of the composites may significantly decrease during degradation, surface modifications are preferred in the combination of PEEK and magnesium. But studies about the biological effects of Mg-containing coatings inside the porous PEEK scaffolds are insufficient.

In this study, PEEK implants with porous structures were prepared via 3D printing, and the hydrophilicity and bioactivity of PEEK materials were further enhanced by surface modification with PDA and further chelation with magnesium ions. To verify whether the porous structural design and functionalized surface modification can promote osseointegration via angiogenesis and osteogenesis, a series of *in vitro* experiments were utilized to investigate the biosafety, biocompatibility, osteogenic-vascular effect, and other bioactivities of the surface-modified porous PEEK scaffolds. The osseointegration of porous PEEK scaffolds in each group was also evaluated through *in vivo* experiments.

2. Methods

2.1. Preparation and surface modification of porous PEEK scaffolds

Porous PEEK scaffolds were manufactured using a 3D printer based on fused deposition modeling. Generally, three types of porous PEEK scaffolds with a pore size of 400 μ m and a porosity of 50% were designed using Materialise 3-Matic software. The scaffolds used for mechanical testing were cube shaped with a side length of 1 cm; the scaffolds used for *in vitro* experiments were disc shaped with a diameter of 14 mm and a height of 2 mm; the scaffolds used for *in vivo* experiments were cylinder

shaped with a diameter of 6 mm and a height of 10 mm. Medical-grade PEEK filaments were extruded into the deposition bin in the 3D printer, and the scaffolds were prepared layer by layer to form previously designed shapes at the temperature of 200 °C. After preparation, a group of PEEK scaffolds were immersed into a reaction solution with 10 mM Tris (hydroxymethyl)aminomethane (Tris), 2 mM dopamine and a pH of 8.5. At 25 °C and protected from light, the reaction continued for 24 h until the inner and outer surfaces of the scaffolds were fully coated with polydopamine. Furthermore, a group of polydopamine-coated scaffolds were immersed into a reaction solution with 10 mM Tris, 50 mg/mL MgCl₂ and a pH of 8.5. This immersion also lasted for 24 h under the same conditions as described above. Finally, all the scaffolds were carefully washed with distilled water 3 times for 5 min each time.

In the following sections, porous PEEK scaffolds without surface modifications are denoted the "PP" group; porous PEEK scaffolds with polydopamine are denoted the "PPD" group; and porous PEEK scaffolds with polydopamine and Mg are denoted the "PPDM" group.

2.2. Characterization of porous PEEK scaffolds

2.2.1. Structural characterization

Microcomputed tomography (Micro-CT, SkyScan 1276, Bruker) was used to detect the structure of porous PEEK scaffolds. Briefly, the porous PEEK scaffolds were placed in the scanning carrier and fixed with tape. The scanning parameters were set as follows: scanning resolution of 8 μm , scanning voltage of 40 kV, and scanning rotation angle of 360° . After scanning, the original data were reconstructed using NRecon 2.0 software. Dataviewer 1.5.6 software was then used to adjust the 2D image stacks. Finally, the images were transferred into VG studio Max 2.1 software to calculate the pore size, filament diameter and porosity in a 3D view (threshold value: -508).

2.2.2. Compression tests

The cubic porous PEEK scaffolds were fixed on the holder of an electronic universal testing machine (WDW20) and compressed in the X-axis and Z-axis directions, separately (Supplementary 1). The compression speed was 0.5 mm/s and the load-displacement curves were automatically recorded until the displacement reached 3.0 mm. Then the load-displacement curves were transformed into stress-strain curves. The maximum stress was taken from the turning point on the curve, and the compressive modulus was calculated from the linear range in the stress-stain curve before the turning point.

2.2.3. Surface characterization

The morphology and elements on the surface of the scaffolds were detected via scanning electron microscopy (SEM; S4800, HITACHI) and energy-dispersive spectroscopy (EDS). Before scanning, the scaffolds were fixed on the microscope stage and sprayed with Pt using an E–1010 ion sputter coater to enhance the electrical conductivity. Then, the surface morphology at magnifications of $100\times$ and $500\times$ was captured and the elements on the surface were detected and labeled. To test the water contact angle of the surface of the scaffolds, 5 μ L distilled water was dropped on the surface of the scaffolds. The contact angle was filmed using a contact angle goniometer and recoded with SCA20 software. Atomic force microscopy (AFM) was used to study the microscopic features of the scaffolds in different groups. The roughness of the surface was analyzed using the AFM data and images.

2.2.4. Mg²⁺ release

Extracts of the scaffolds in the PPDM group were prepared according to the national standard GB/T 16886.12–200 and the ${\rm Mg}^{2+}$ release curves of the scaffolds were measured [27]. The scaffolds were immersed in D-Hank's solution (${\rm Mg}^{2+}$ free) at a mass-volume ratio of 1 g:10 mL for 15 days. The solutions were refreshed every 2 days and the ${\rm Mg}^{2+}$ concentrations were measured via inductively coupled plasma emission spectrometry (ICP-OES). Then the accumulative release curve

of Mg^{2+} was plotted to observe the ion release characteristics of scaffolds in the PPDM group.

2.3. In vitro experiments

2.3.1. Coculture of cells and the scaffolds

MC3T3-E1 cell and HUVEC lines were purchased from ATCC. MC3T3-E1 cells were cultured in complete $\alpha\text{-MEM}$ ($\alpha\text{-MEM}$ with 1% penicillin, 10% fetal bovine serum), and HUVECs were cultured in complete ECM medium (ECM with 1% penicillin, 1% endothelial cell growth supplementation factor, 10% fetal bovine serum). All the cells were incubated in an incubator at a temperature of 37 °C, with a CO2 concentration of 5%, and 95% humidity.

Before coculture with cells, the scaffolds used for *in vitro* experiments were sterilized by Co⁶⁰ irradiation. In this study, there were two types of cocultures of scaffolds and cells; in one, cells were seeded directly on the surface of scaffolds (direct contact), and in the other, cells were seeded on the bottom of the medium and the scaffolds were set on the chamber above the cells (indirect contact). During coculture, the medium was refreshed every 2 days.

2.3.2. Cell proliferation and apoptosis assay

MC3T3-E1 cells and HUVECs were cocultured with porous PEEK scaffolds in different groups by direct contact. Cell proliferation was detected with cell counting kit 8 (CCK-8; IC-1519, BioCytoSci) after coculture for 24 h, 48 h and 72 h. Briefly, at 0 h and 2 h after addition of CCK-8 reagent to a 10% volume of the medium, the absorbance at 450 nm (Ab450) was measured using a microplate reader (Biotek Synergy H1), and the proliferation curves of cells in different groups were plotted. Apoptosis of the cells was detected via Annexin V-FITC/propidium iodide (PI) double staining and flow cytometry. After coculture for 48 h, the cells were collected from each group and resuspended in 1 mL of phosphate-buffer saline (PBS) with 50 μ L of Annexin V-FITC and 15 μ L of PI. After 30 min of incubation in the dark, the samples were assessed via flow cytometry (FACS Vantage SE, BD Biosciences).

2.3.3. Cell adhesion and morphology on the surface of scaffolds

MC3T3-E1 cells and HUVECs at a density of 1×10^5 cells/mL were seeded on the surface of the scaffolds in different groups. After coculture for 24 h by direct contact, the cells were fixed using 4% polyparaformaldehyde for 30 min and then stained with DAPI to visualize the nuclei. An inverted fluorescence microscope (Axio Observer, Carl Zeiss) was used to capture the images of nuclei on the surface of the scaffolds, and nuclei were counted using Image-Pro Plus 6 software. Cell morphology was observed via SEM. Cells seeded on the surface of scaffolds were fixed using 2.5% glutaraldehyde and dehydrated by gradient alcohol. After critical point drying with a critical dryer, the samples were sprayed with Pt and cell images were captured via SEM at magnifications of 200 \times and 1000 \times .

2.3.4. Immunofluorescence staining of cells

Due to the shape limitation of porous PEEK scaffolds and the strong light transmission of PEEK material under fluorescence microscopy, it was difficult for us to observe fluorescence in cells directly cocultured on the surface of porous PEEK scaffolds; thus, the immunofluorescence staining assays were performed under coculture under indirect contact conditions only. MC3T3-E1 cells and HUVECs and scaffolds of different groups were cocultured by indirect contact for 24 h as described in 2.3.1. Cells in the medium were then fixed with 4% paraformaldehyde and incubated with primary antibody against vinculin (ab130007, Abcam) overnight at 4 °C. The next day, the cells were washed with PBST (1 \times PBS with 0.1% Tween) to remove unconjugated primary antibody and incubated with a fluorescent secondary antibody (Ab150115, Abcam) and for 1 h. Then, FITC phalloidin was added to stain F-actin, and DAPI was added to stain nuclei. Fluorescence images were captured via fluorescence microscope under laser excitation, and quantification of

fluorescence intensity was performed using Image-Pro Plus 6 software. After coculture for 48 h, immunofluorescence staining of EMCN and CD31 in HUVECs was also performed according to the above method.

2.3.5. Quantitative real-time PCR

MC3T3-E1 cells were cocultured with scaffolds in each group in osteogenic induction medium (complete medium with 10 mM sodium β-glycerophosphate, 10 nM dexamethasone, and 50 μg/mL ascorbic acid) via direct and indirect contact for 3 days. The expressions levels of the osteogenesis-related genes, bone morphogenetic protein 2 (Bmp2), runt-related transcription factor 2 (Runx2), osteopontin (Opn), osteocalcin (Ocn), alkaline phosphatase (Alp), and collagen type 1 (Col1) were evaluated using quantitative real-time PCR. Briefly, total RNA was extracted from MC3T3-E1 cells in different groups using an RNA extraction kit (Omega Bio-Tek). The RNA was then transformed into cDNA with a PrimeScriptTM RT master mix kit (Takara). Real-time PCR was performed by using a perfectstart SYBR Green qPCR master mix kit (Omega Bio-Tek) and the CFX96 real-time PCR detection system. The primers for the genes above are listed in Supplementary 2, and the housekeeping gene was GAPDH.

2.3.6. Western blotting assay

HUVECs were cocultured with different scaffolds via direct and indirect contact for 48 h MC3T3-E1 cells were cocultured as described in 2.3.5 for 7 days. Then cells in different groups were lysed in radio-immune precipitation assay (RIPA) buffer and the total protein was collected. The total proteins in each sample were quantified using a BCA Protein Assay Kit (Thermo Scientific, 23227) and mixed with loading buffer and then were loaded onto the SDS-PAGE gels. Approximately 20 μg of total protein loading sample was added to each well. After the proteins were separated via electrophoresis, they were then transferred to PVDF membranes. The membrane containing proteins was incubated with primary antibodies at 4 $^{\circ} \text{C}$ overnight and a secondary antibody for 1 h. OPN, RUNX2, Osterix, and COL1 protein in MC3T3-E1 cells and CD31 and EMCN protein in HUVECs were visualized using ECL reagents (IC-8001, BioCytoSci). The categories of all antibodies used in this study are shown in Supplementary 3.

2.3.7. ALP and Alizarin red staining of MC3T3-E1 cells

MC3T3-E1 cells were cocultured as described in 2.3.5. ALP staining was performed using a BCIP/NBT staining kit (C3206, Beyotime) after 3 and 7 days. Calcium nodules were stained with Alizarin red (C0148S, Beyotime) after 14 and 21 days. Briefly, cells were fixed with 4% paraformaldehyde for 15 min and immersed in dyeing working solution for 30 min. Excess stain was removed by washes with distilled water. The gross appearance of cells was captured using a stereomicroscope (Leica S6E) and the staining details were observed via optical microscopy.

2.3.8. Scratch wound healing and tubule formation assays of HUVECs

HUVECs were cocultured with scaffolds by indirect contact. When cell confluence reached 100%, straight lines through the middle of the cells were scratched in each well. Then the complete medium was replaced with serum-free medium. After 0 h and 12 h, images of the scratches were taken with an inverted microscope. The average width of the scratches was measured using ImageJ 1.51 software, and the scratch wound healing rates were calculated.

A tubule formation assay on the Matrigel (No.354234, Corning) was used to investigate the tube-formation ability of HUVECs after cocultured with different scaffolds. HUVECs were cocultured with scaffolds by direct contact for 48 h, and then, the cells seeded on the scaffolds were resuspended and diluted to a density of 2×10^4 . Then $100~\mu L$ of the cell suspension was added to each well of a 48-well plate coated with Matrigel. After 6 h, images were captured with an inverted microscope and analyzed using ImageJ 1.51 software.

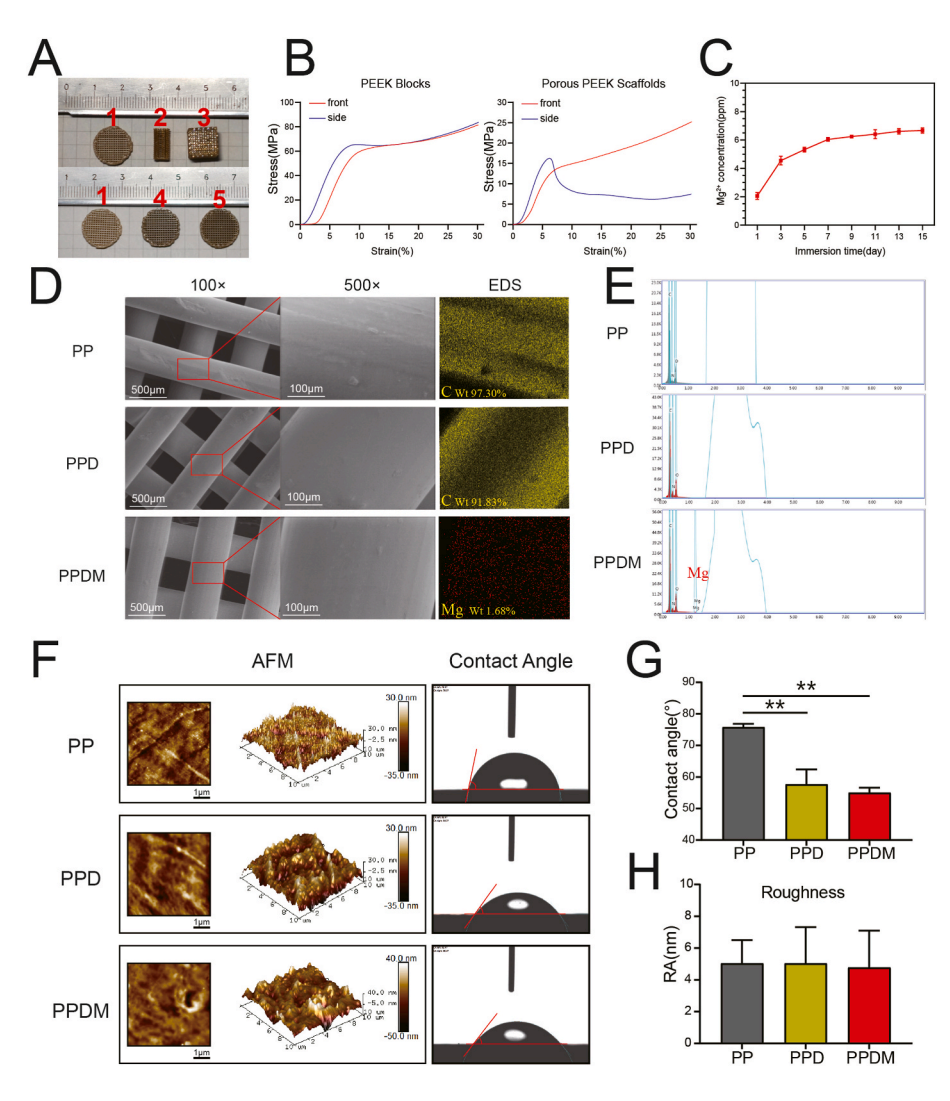


Fig. 1. Characterization and surface analysis of the scaffolds. A) Different porous PEEK scaffolds prepared for *in vitro* (1,3) and *in vivo* (2) experiments and porous PEEK discs of in the PP (1), PPD (4), and PPDM (5) groups. B) Stress-strain curves of porous PEEK scaffolds and PEEK blocks with different orientations. C) Accumulative Mg2+ release in the PPDM group. D) Surface morphologies and elements of porous PEEK scaffolds in different groups examined by SEM and EDS. E) Peaks of different elements on the surface of the PP, PPD and PPDM scaffolds examined by EDS. F) Surface micromorphologies and water contact angles of the scaffolds. G) Water contact angles and H) surface roughness in different groups were statistically analyzed, n=5; **p<0.01.

2.4. In vivo experiments

2.4.1. Construction of bilateral femoral condylar bone defects and scaffold implantation in rabbits

Thirty-six healthy male New Zealand White rabbits aged 6-8 weeks and weighing 2.5-3.5 kg were selected from the Experimental Animal Center. During the experiments, all rabbits were treated well according to the ethical and welfare review of experimental animals (IACUC-20200501). The rabbits were randomly numbered and divided into three groups (PP, PPD, and PPDM groups) according to the implanted porous PEEK scaffolds. The animal model of femoral condylar bone defects was established according to the published references [28]. Briefly, the rabbits were anesthetized by intramuscular injection with 30 mg/kg pentobarbital sodium and 20 mg/kg xylazine hydrochloride. Then the limb shin was prepared and an incision along the femoral shaft was made to expose the femoral condyle. A cylinder-shaped bone defect of 6 mm in diameter and 10 mm in depth was made with a bone drill in the middle of the epiphysis. Subsequently, for in vivo experiments, porous PEEK scaffolds from different groups were randomly implanted in both sides of the femoral condyle, and the rabbits were individually identified by ear tags.

2.4.2. Vascular perfusion

At 2, 4, and 8 weeks after implantation for, two of the rabbits in each group were randomly selected to perform microvascular perfusion as described in a previous study [29], and four femoral condyle samples

were preserved. Briefly, the rabbits were anesthetized and the abdominal hair was removed. The skin, subcutaneous fascia, abdominal muscles and peritoneum were incised along the median abdominal incision to expose the abdominal cavity. The abdominal aorta and inferior vena cava were exposed and bluntly separated. The proximal ends of the abdominal aorta and inferior vena cava were closed with a vascular clamp, and a 1.5-mm diameter infuser hose was placed and secured in the distal end of the abdominal aorta, followed by ligation of the proximal ends of the abdominal aorta and inferior vena cava, clipping of the inferior vena cava, and drainage of blood and perfusion fluid with a suction device. After successful establishment of perfusion access to the lower extremities, the experimental rabbits were euthanized. The lower extremity vessels were continuously perfused with saline with a sodium heparin concentration of 400 U/L until the venous outflow was clear. The lower extremity vessels were subsequently perfused with 10% paraformaldehyde and the hind limb was fixed. MV-117 perfusion solution was configured according to the MICROFIL® perfusion solution instructions, and 50 mL of the solution was used to perfuse the lower extremity vessels of each rabbit with an automatic syringe pump at a rate of 2 mL/min. After perfusion, the rabbit femurs were harvested, fixed with 4% paraformaldehyde for 72 h, and then decalcified with 10% EDTA solution for 2 months.

2.4.3. Micro-CT assessment

At 4, 8, and 12 weeks after implantation, two of the rabbits in each group were sacrificed at each time point and the femurs were harvested

Table 1 Structural properties of the scaffolds.

Pore size (µm)	429 ± 37
Porosity (%)	45.8 ± 3.1
Elastic modulus in the X axis (MPa)	376 ± 17
Elastic modulus in the Z axis (MPa)	407 ± 25
Compressive strength in the X axis (MPa)	14 ± 2
Compressive strength in the Z axis (MPa)	18 ± 3

and fixed. To investigate the bone and vascular ingrowth inside different porous PEEK scaffolds, all samples were scanned using micro-CT. The parameters were as follows: scanning resolution of 8 μm , ray source voltage of 80 kV; current of 200 μA , and scanning rotation angle of 360°. The scanned images were subsequently reconstructed using NRecon reconstruction software and analyzed using VG studio max 2.1 software. The region of interest was set as a 6 mm diameter by 10 mm high cylinder for all samples and bone 3D images or vascular 3D images inside porous PEEK scaffolds from different groups were constructed by the same threshold segmentation (bone>226, vascular>343). Bone volume fraction (the ratio of bone volume to total volume, BV/TV), blood vessel volume fraction (the ratio of blood vessel volume to total volume, BVV/TV), trabecular thickness and vascular diameter were calculated and statistically analyzed.

2.4.4. Histological evaluation

After being scanned via micro-CT, all samples were dehydrated and polymerized to obtain hard-tissue sections. Briefly, the samples were thoroughly dehydrated using gradient alcohol and xylene and subsequently encapsulated in a plasticizer containing methyl methacrylate and dibutyl phthalate. Then, 150 mm-thick sections were made by the hard tissue slicer (Leica Microtome, Wetzla, Germany) and polished with polishing papers. The sections with vessel perfusion were observed via fluorescence microscopy with excitation light of wavelength between 430 and 460 nm. The diameters of vessel inside the scaffolds were manually measured by using Image pro plus software and the mean blood vessel diameter was statistical analyzed. The density of blood vessel was estimated by calculating ratio of red vessel area to the total scaffolds area. For sections without vessel perfusion, Van Gieson's staining was conducted by Stevenel's blue and picric acid magenta dye solution. The optical microscope (Olympus) was used to observe sections after staining. The area of bone (stained with dark red) inside the scaffolds was measured and BV/TV was estimated by calculating ratio of bone area and total scaffolds area. The bone-implant contact (BIC, the percentage of implant perimeter showing a direct bone-to-implant contact without any intervening soft-tissue layers) was measured by calculating the ratio of the length of bone tissue which is directly contacted with the scaffolds to the total length of the surface of scaffolds.

2.5. Statistical analysis

The above experiments were repeated at least three times independently, and the results are shown as the form of mean \pm standard deviation. All the experimental results were plotted and statistically analyzed using GraphPad Prism (version 8.0) software. Student's t-test was used to compare two groups and multiple groups were compared by one-way analysis of variance (ANOVA) and Tukey's post-hoc multiple test was used to compare the differences between groups. Differences were considered statistically significant when p<0.05.

3. Results

3.1. Characterization of scaffolds in different groups

Porous PEEK scaffolds were fabricated by FDM (Fig. 1A) and their structural parameters are shown in Table 1. The porosity of PEEK scaffolds was 45.8% \pm 3.1%, the pore size was 429 \pm 37 μm and the pore connectivity was 100%. The stress-stain curves of PEEK scaffolds and PEEK blocks are shown in Fig. 1B. The compression modulus of porous PEEK scaffolds in the X-axis and Z-axis directions were 376 \pm 17 MPa and 407 \pm 25 MPa, respectively, which were similar to the modulus of cancellous bone (0.1–4.5 GPa [30]). The compression modulus of the PEEK blocks was 1183 \pm 74 MPa.

The surface morphology of PEEK scaffolds before and after surface modification was observed by SEM and AFM. As shown in Fig. 1D, the surface morphology of porous PEEK scaffolds in the three groups did not differ significantly at 100x and 500x magnification, and additional Mg was found on the surface of PPDM scaffolds compared to scaffolds in the PP and PPD groups (Fig. 1E). The surface micromorphology and roughness of PEEK scaffolds were detected by AFM (Fig. 1F), and no significant difference was found among the three groups was found (Fig. 1H). However, the water contact angles in the PPD and PPDM groups were significantly smaller than that in the PP group (Fig. 1G). In the PPDM group, Mg²⁺ was released sustainably in two weeks, and the release was more obvious in the first 7 days (Fig. 1C).

3.2. Biosafety of PDA and Mg coatings

Proliferation curves clearly showed that MC3T3-E1 cells and

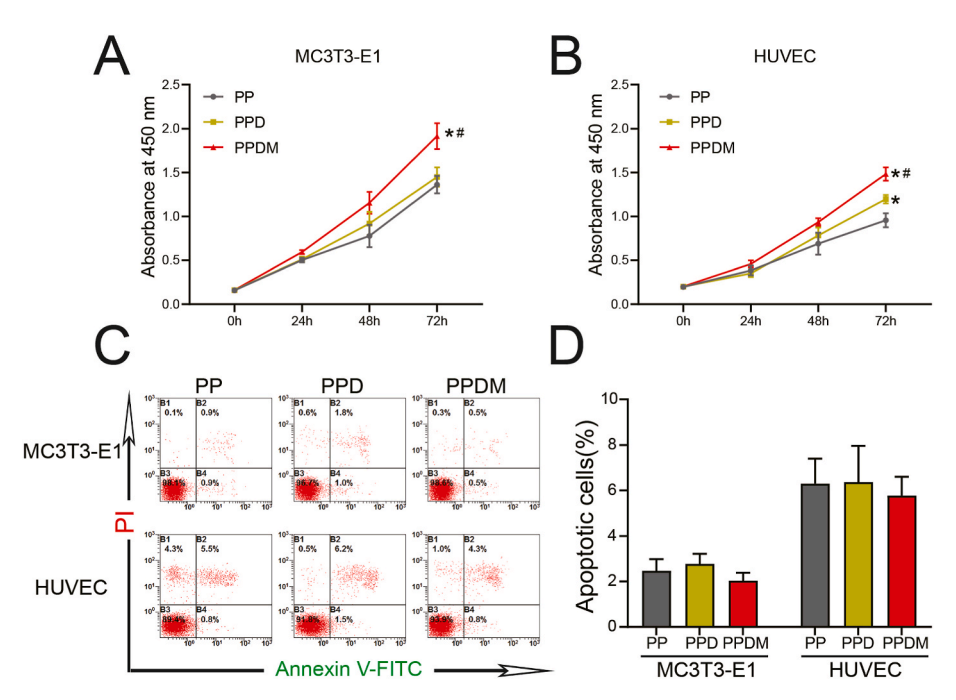


Fig. 2. Proliferation and apoptosis of cells cocultured with different scaffolds. A) MC3T3-E1 cells and B) HUVECs proliferation after 0 h, 24 h, 48 h, 72 h determined by CCK-8 assays, n=5; *p<0.05 compared with the PP group; *p<0.05 compared with the PPD group. C) Cell apoptosis detected after 48 h. D) Statistical analysis of apoptosis rates. n=3, *p<0.05.

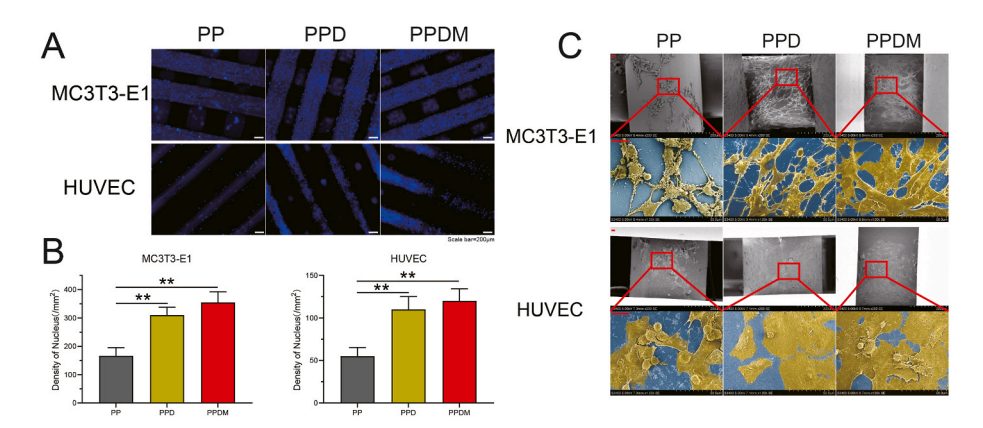


Fig. 3. Adhesion of HUVECs and MC3T3-E1 cells on the surface of porous PEEK scaffolds in each group. A) Nuclei distribution of HUVECs and MC3T3-E1 cells on the surface of the scaffolds. Scale bar = $200 \ \mu m$. B) Statistical analysis of the density of cell nuclei, n = 3; **p < 0.01. C) Morphology of cells adhering to the surface of the scaffolds determined by SEM. Cells are highlighted in yellow in contrast to the blue substrate.

HUVECs on the surface of the scaffolds in the PPDM group grew faster than those cultured on scaffolds in the PP and PPD groups (Fig. 2A and B). The apoptosis results of cocultured MC3T3-E1 cells and HUVECs was detected by flow cytometry, and the results are shown in Fig. 2C. No significant difference was found among the three groups (Fig. 2D).

3.3. Cell adhesion was enhanced by surface modification of porous PEEK scaffolds

The number of adherent cells on the surface of scaffolds in each group was observed by nuclear fluorescence staining. The filaments of the PEEK scaffolds were light blue and the cell nuclei were dark blue under laser excitation (Fig. 3A). After statistical analysis, the density of cell nuclei in the PPDM and PPD groups was significantly higher than in the PP group, while there was no significant difference between the PPD and PPDM groups. In the SEM images, MC3T3-E1 cells and HUVECs in the PP group were clearly clumped and bulged after adhesion, indicating that the cells did not adhere firmly to unmodified surface, while cells in

the PPD and PPDM groups displayed a spreading pattern (Fig. 3C). In addition, the spreading area of MC3T3-E1 cells in the PPDM group was larger than that in the PPD group but the spreading area of HUVECs was similar between the PPD and PPDM groups.

MC3T3-E1 cells and HUVECs were also cocultured with different groups of porous PEEK scaffolds by indirect contact. The spreading area of cells around the scaffold and the expression of vinculin were examined by immunofluorescence staining (Fig. 4A and D). The average spreading area of MC3T3-E1 cells in the PPDM group was larger than that in the PP group and PPD group (Fig. 4B). For cocultured HUVECs, no significant difference was found among the groups (Fig. 4E). The expression of vinculin, an adhesive patch protein in HUVECs and MC3T3 cells, was significantly increased in the PPDM group compared to the PP and PPD groups (Fig. 4C and F).

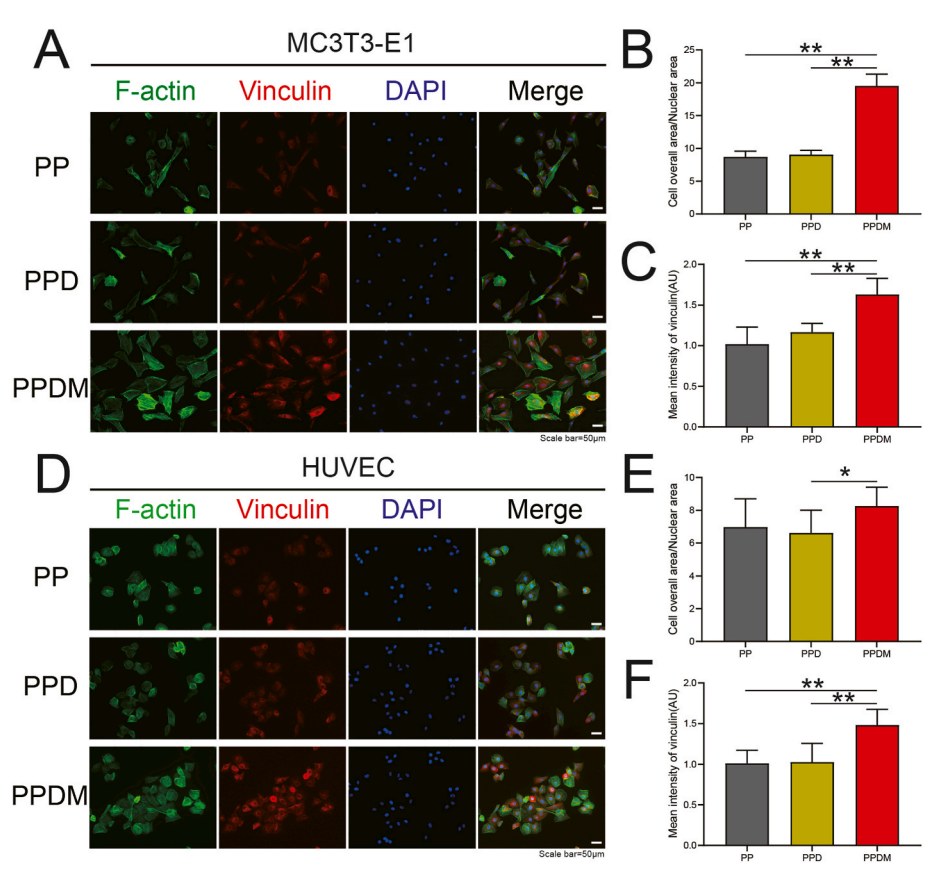


Fig. 4. Adhesion of HUVECs and MC3T3-E1 cells cocultured with scaffolds by indirect contact. A) Immunofluorescence staining of F-actin and vinculin in MC3T3-E1 cells after 24 h. Scale bar = 50 μ m. B) The ratio of total cell area to nucleus area (CN ratio) and C) fluorescence intensity (FI) of vinculin in MC3T3-E1 cells were calculated and analyzed. D) Immunofluorescence staining of F-actin and vinculin in HUVECs after 24 h. Scale bar = 50 μ m. E) CN ratio and F) FI of vinculin in HUVECs were statistically analyzed. n = 3; *p < 0.05; **p < 0.01.

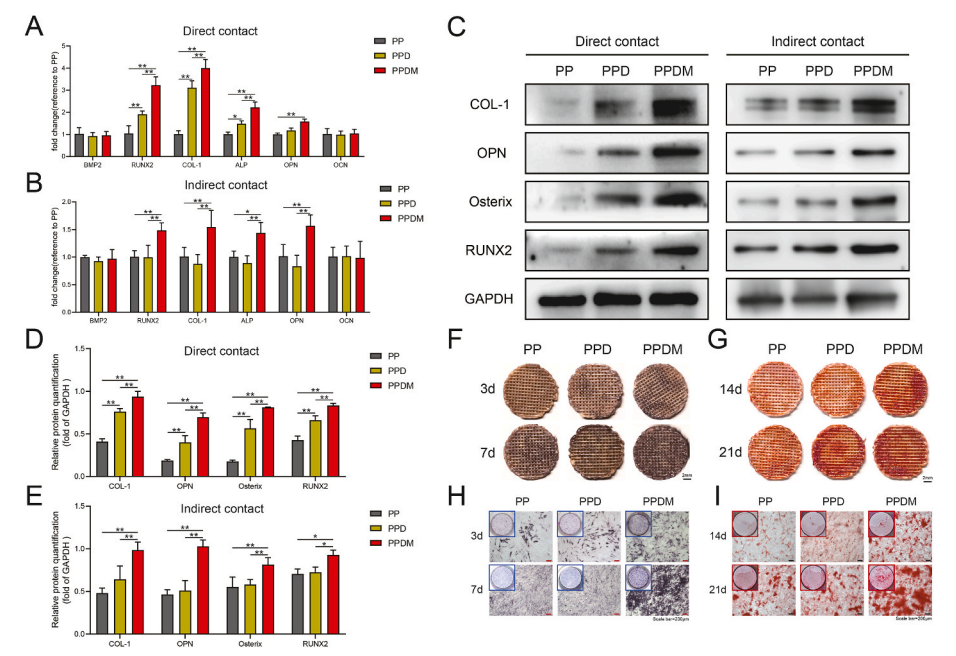


Fig. 5. Effect of different scaffolds on osteogenic differentiation and mineralization of MC3T3-E1 cells. A) Relative mRNA expression of osteogenesis-related genes (Bmp2, Runx2, Col-1, Alp, Opn, Ocn) in MC3T3-E1 cells cocultured with the scaffolds by direct contact and B) indirect contact after 3 d. C) Relative expression of osteogenesis-related proteins (COL-1, OPN, Osterix, RUNX2) after 7 d. D) Grayscale analysis of Western blot bands after direct contact and E) indirect contact culture. F) ALP staining of MC3T3-E1 cells cocultured by direct contact and H) indirect contact after 3 d and 7 d. G) Alizarin red staining of cells cultured via direct contact and I) indirect contact after 14 d and 21 d. Scale bar = 200 μ m n = 3; *p < 0.05; **p < 0.01.

3.4. Effects of scaffolds in each group on osteogenic differentiation of MC3T3-E1 cells

First, the osteogenic differentiation of MC3T3-E1 cells was examined at the transcriptional level. After coculture by direct contact, the expression of the *Runx2*, *Col1*, and *Alp* genes was significantly higher in the PPDM and PPD groups than in the PP group (Fig. 5A). After coculture

by indirect contact, the *Rumx2, Col1, Alp,* and *Opn* genes were upregulated in the PPDM group compared with the PP and PPD groups, but the difference between the PP and PPD groups was not significant (Fig. 5B). For the *Bmp2* and *Ocn* genes, no significant difference was found among the three groups. Furthermore, osteogenesis-related proteins in MC3T3-E1 cells were detected (Fig. 5C). According to grayscale analysis, the relative protein expression levels of COL1, OPN, Osterix, and RUNX2 in

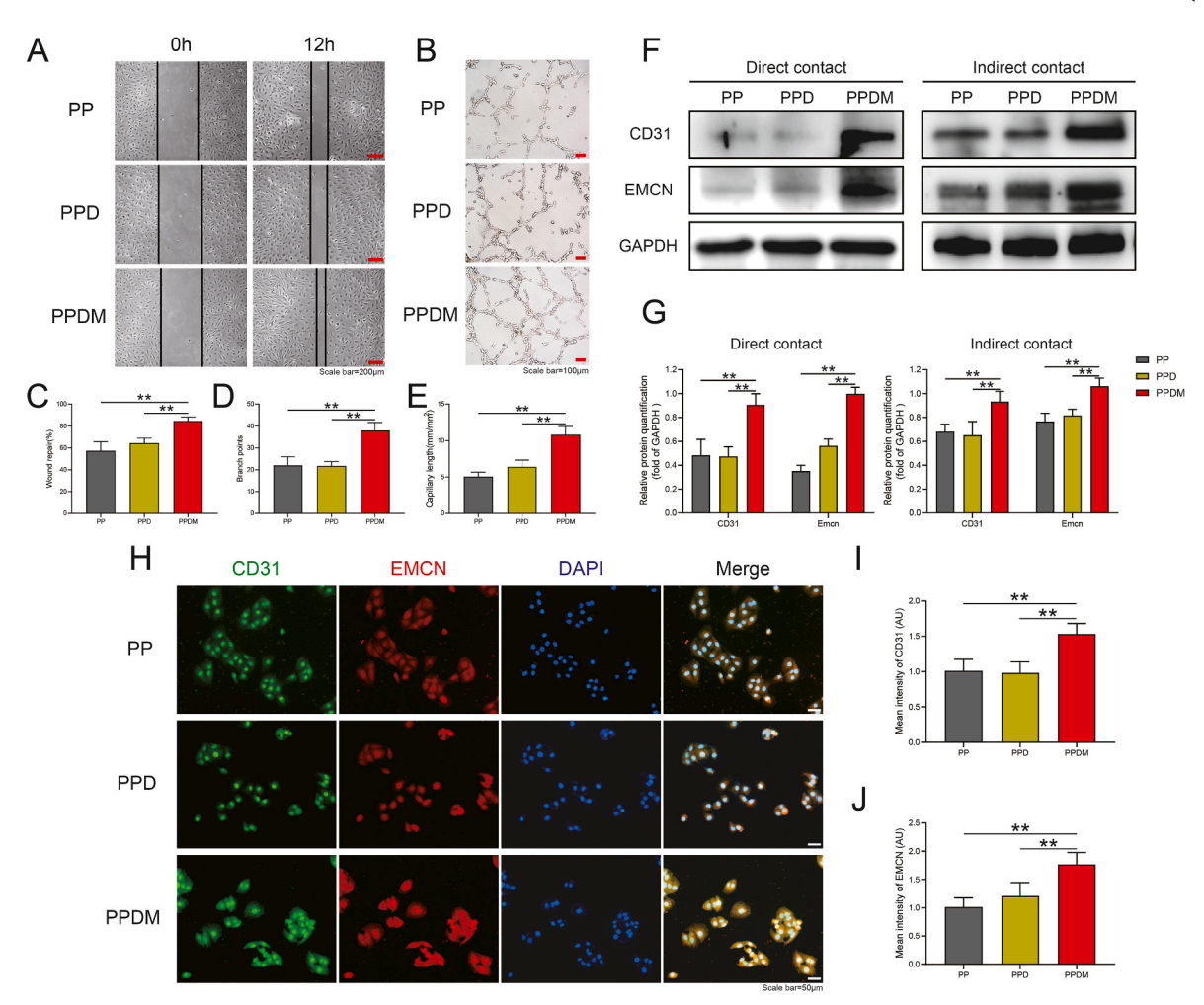


Fig. 6. Effect of different scaffolds on HUVECs migration and angiogenesis. A) Scratch wound healing of HUVECs cocultured with different scaffolds after 12 h, scale bar = $200 \, \mu m$. B) Tubule formation of HUVECs; scale bar = $100 \, \mu m$. C) Statistical analysis of wound healing. D) Quantitative analysis of branch points and E) average capillary length. F) Relative CD31 and EMCN protein expression in HUVECs cocultured by direct and indirect contact with different scaffolds. G) Grayscale analysis of CD31 and EMCN protein expression. H) Immunofluorescence staining of EMCN and CD31 in HUVECs. Scale bar = $50 \, \mu m$. I) The FI of CD31 and J) EMCN in HUVECs were analyzed. n = 3; **p < 0.01.

the PPDM group were notably higher than those in the PP and PPD groups regardless of whether the cells were cocultured by direct or indirect contact. A difference in osteogenesis-associated proteins was only detected between the PPD group and the PP group after coculture by direct contact (Fig. 5D and E).

Finally, the effects of different groups of porous PEEK scaffolds on the early osteogenic differentiation of MC3T3-E1 cells were visualized by ALP staining, and the effect of different groups of porous PEEK scaffolds on osteogenic mineralization of MC3T3-E1 cells was detected by alizarin red staining. At Day 3, the ALP staining on the scaffold surface in the PPDM group could already be seen to be deeper than that in the PP and PPD groups, and at Day 7, the ALP staining in the PPDM group further deepened, while the difference in ALP staining between the PP and PPD groups was not significant (Fig. 5F). At Day 14, MC3T3-E1 cells on the surface of the scaffold in the PPDM group had started to form deep-stained red calcium nodules, while staining in the PP and PPD groups was not obvious. At Day 21, a clear distribution of calcium nodules was observed on the scaffold surface in both the PPD and PPDM groups, while those in the PP group were still not obvious (Fig. 5G). After coculture of MC3T3-E1 cells with scaffolds in different groups culture dishes for 3 days, the ALP staining in the PPDM group was darker than that in the PP and PPD groups, and at Day 7, the ALP staining in all groups was further deepened, while the staining in the PPDM group was still darker than that in the PP and PPD groups (Fig. 5H). At Day 14,

mineralized nodules began to appear in the cells in the PPDM group, while calcium nodules were not evident in the PP and PPD groups. At Day 21, calcium nodules also started to appear in the cells in the PP and PPD groups, but at this time in the PPDM group, large calcium nodules could be observed in the culture dish and under the microscope (Fig. 51).

3.5. Effects of scaffolds in each group the migration and angiogenesis of HUVECs

The results of scratching experiments under indirect contact coculture conditions between HUVECs and different groups of porous PEEK scaffolds are shown in Fig. 6A. HUVECs obtained significant healing by migration in the PP group, PPD group and PPDM group within 12 h. Statistical analysis of the results showed that the healing effect in the PPDM group was significantly higher than that in the PP and PPD groups, while there was no significant difference in the healing effect of cell migration between the PP and PPD groups (Fig. 6C). In the tubule formation experiment, HUVECs in the PPDM group were able to form obvious tubular structures at 6 h, while cells in the PP and PPD groups only formed a large number of vascular branching structures with discontinuous tubular walls (Fig. 6B). According to statistical analysis, both the number of vascular branch nodes and the mean vessel length in the PPDM group were higher than those in the PP and PPD groups, while there was no significant difference between the PP and

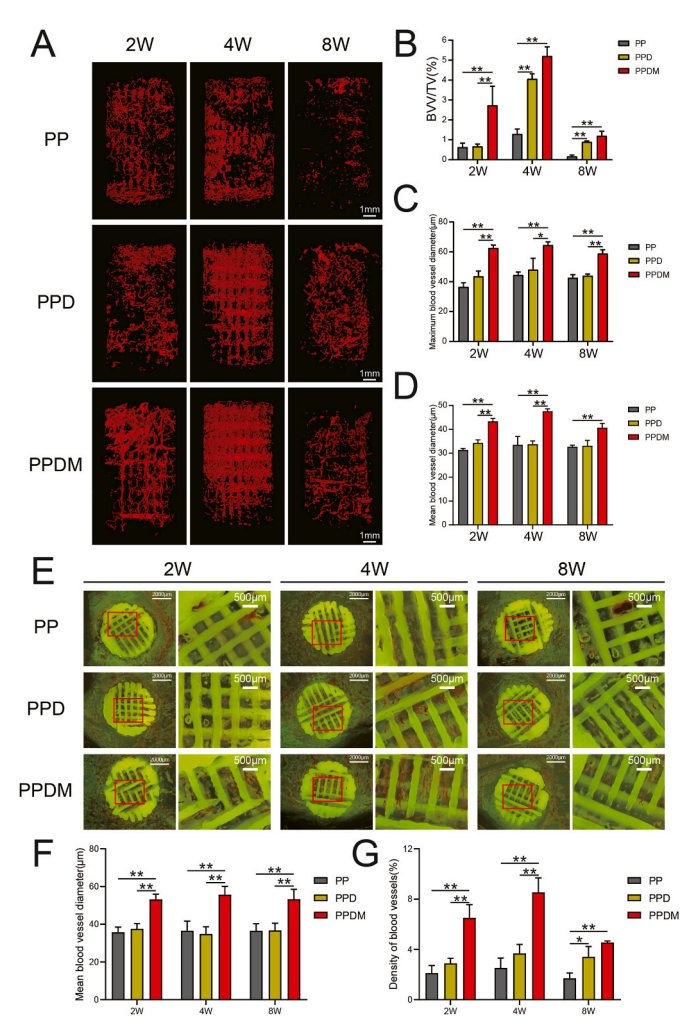


Fig. 7. Vessel ingrowth in porous PEEK scaffolds in different groups. A) 3D reconstructed images of the internal vessels detected by micro-CT in porous PEEK scaffolds at 2, 4, 8 weeks after implantation. B) Quantitative analysis of the vessel volume, C) maximum vessel diameter and D) mean vessel diameter inside the scaffolds. E) Histological images of blood vessels inside the scaffolds. F) Mean vessel diameter and G) vessel density in histological sections were quantitatively analyzed. $n=4;\ ^*p<0.05;\ ^**p<0.01.$

PPD groups.

Western blotting and immunofluorescence staining results demonstrated the effects of different groups of porous PEEK scaffolds on the expression of CD31 and EMCN, vascular markers associated with angiogenesis in HUVECs. The protein expressions levels in HUVECs after coculture with different groups of scaffolds in direct and indirect contact for 48 h are shown in Fig. 6F. Under direct contact coculture conditions, the expression of CD31 and EMCN proteins was the highest in the PPDM group among the groups. Grayscale analysis showed that expression was significantly higher the PPDM group than in the PP and PPD groups, while the differences in protein expression between the PP and PPD groups were not significant. The results of indirect contact coculture were similar to those of direct contact coculture, and grayscale analysis showed that expression was significantly higher in the PPDM group than in the PP and PPD groups (Fig. 6G). The results were also confirmed by immunofluorescence staining. Compared to the PP and PPD groups, brighter CD31 and EMCN fluorescence was observed in the PPDM group (Fig. 6H). The immunofluorescence intensity of the two proteins in each group of cells was counted, and the fluorescence intensity of CD31 protein and EMCN protein in the PPDM group was significantly higher than that in the PP and PPD groups.

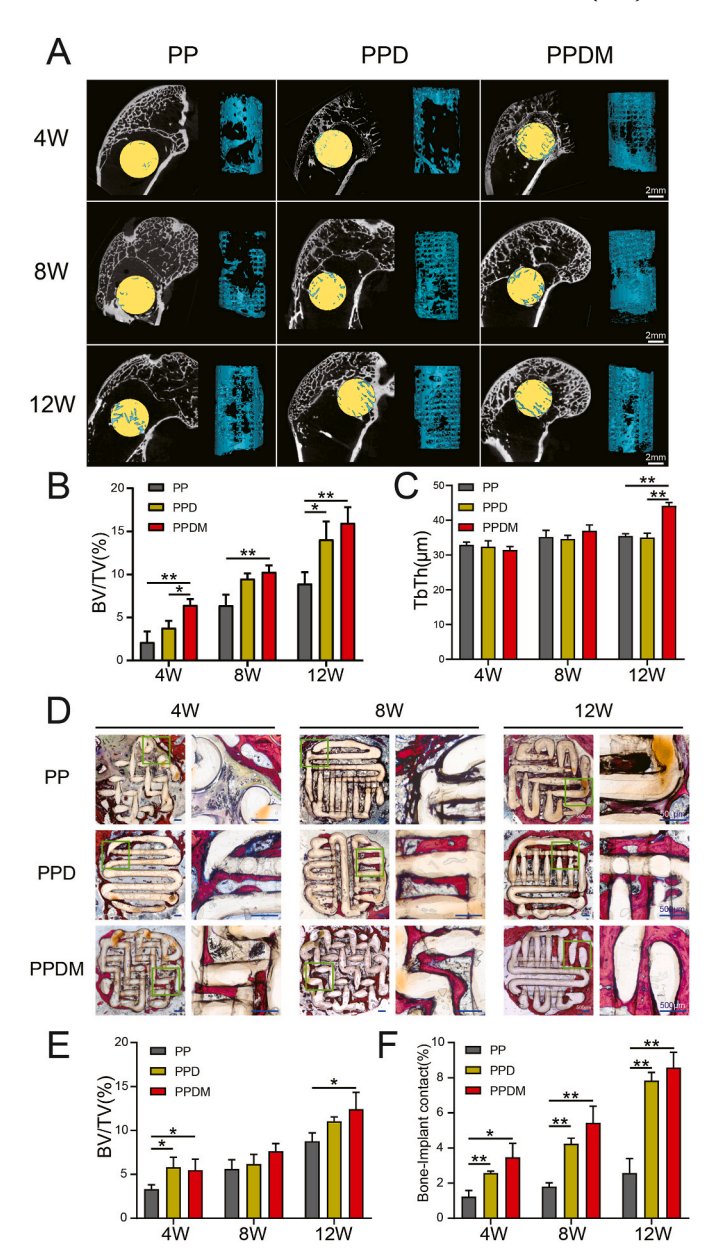


Fig. 8. Osseointegration of different porous PEEK scaffolds. A) Bone ingrowth in the scaffolds determined by micro-CT at 4, 8, 12 weeks after implantation. B) Quantitative analysis of the bone volume and C) bone trabecular thickness (TbTh). D) Histological images of bone inside the scaffolds. E) Bone volume and F) bone-implant contact were calculated and statistically analyzed. $n=4;\ ^*p<0.05;\ ^*p<0.01.$

3.6. PDA and Mg coating enhanced the angiogenesis induction capacity of porous PEEK scaffolds in vivo

A large number of vessels were observed in the three groups of porous PEEK scaffolds two weeks after *in vivo* implantation, with a further increase in vessel volume at four weeks but a rapid decrease at eight weeks, a trend evident in all three porous PEEK scaffold groups. Two weeks after implantation, more mature and continuous vessels had formed inside the PPDM group, whereas the PP and PPD groups had less complete and continuous vessel morphology and exhibited a state of neovascularization. Four weeks after implantation, a large amount of interrupted and branched neovascularization was observed in all three groups of porous PEEK scaffolds. The vascular morphology inside the porous PEEK scaffolds at 8 weeks of implantation was more fragmented (Fig. 7A). In terms of vessel volume, BVV/TV was significantly higher in

the PPDM group than in the PP and PPD groups at 2 weeks after implantation and there was no significant difference between the PP and PPD groups. At 4 and 8 weeks after implantation, the BVV/TV in both the PPD and PPDM groups was higher than that in the PP group and there was no significant difference between the PPD and PPDM groups (Fig. 7B). Further analysis revealed that the mean and maximum diameter of the vessels was higher in the PPDM group than in the PP and PPD groups at 2, 4, and 8 weeks after implantation, while the differences between the PP and PPD groups were not significant (Fig. 7C and D).

In hard tissue sections, the vessels could be directly observed inside the porous PEEK scaffolds. In contrast to the fluorescent background, the porous PEEK scaffold was yellow-green, and the vessels inside the aperture are shown in red. For vessels parallel to the section plane, the intact shape and branching could be observed, and vessels perpendicular to the section plane presented a circular-like cross-section. At 2 weeks after implantation, small, interrupted neovascularization was observed in the PP and PPD groups, while clusters of vessels were observed in the pores of the porous PEEK scaffolds in the PPDM group; at 4 weeks after implantation, large numbers of red clusters of neovascularization were observed in the pores of the porous PEEK scaffolds in both the PPD and PPDM groups, while the vessels in the PP group remained more dispersed; at 8 weeks after implantation, the number of vessels in the pores of the porous PEEK scaffolds was significantly reduced in all three groups (Fig. 7E). Statistical analysis showed that the mean vessel diameter in the PPDM group was higher than that in the PP and PPD groups at all time points (Fig. 7F). The vessel density in the PPDM group was significantly higher than that in the PP and PPD groups at 2 and 4 weeks after implantation, but the difference in vessel density between the PPDM and PPD groups was no longer significant at 8 weeks after implantation (Fig. 7G).

3.7. PDA and Mg coating improved osseointegration of porous PEEK scaffolds in vivo

The results of the 3D reconstruction of bone ingrowth inside the porous PEEK scaffold are shown in Fig. 8A. At 4 weeks after implantation, bone ingrowth was concentrated at the edge of the scaffold, and as the implantation time increased, bone ingrowth gradually penetrated deeper inside the porous PEEK scaffold. In terms of bone volume fraction, bone ingrowth inside the porous PEEK scaffold increased with the duration of implantation in all three groups. At 4 weeks after implantation, the PPDM group had significantly more internal bone growth into the porous PEEK scaffold than the PP and PPD groups, while there was no significant difference between the PP and PPD groups. At 8 weeks after implantation, the gap in bone length entry within the three scaffold groups narrowed, with bone length in the PPDM group slightly greater than that in the PP group, and no significant difference was observed between the PPDM and PPD groups or the PPD and PP groups. At 12 weeks after implantation, BV/TV was significantly higher in the PPD and PPDM groups, while the difference between the PPD and PPDM groups was not significant (Fig. 8B). In terms of bone trabecular thickness (TbTh), there was no significant difference in trabecular thickness of bone tissue inside the three groups of scaffolds at 4 and 8 weeks after implantation, but at 12 weeks after implantation, bone trabecular thickness was higher in the PPDM group than in the PP and PPD groups (Fig. 8C).

Hard tissue sections showed that bone ingrowth within the porous PEEK scaffold at 4 weeks after implantation was concentrated at the edge of the scaffold, consistent with the results of micro-CT analysis. At 8 weeks after implantation, bone ingrowth was observed in the deep part of the porous PEEK scaffold in the PPD and PPDM groups, while bone ingrowth in the PP group remained concentrated at the edge of the porous PEEK scaffold. At 12 weeks after implantation, the edges of the triple porous PEEK scaffold were already heavily encapsulated with bone tissue (Fig. 8D). Under high magnification, it was observed that the contact between the bone tissue and the PEEK scaffold surface was

tighter in the PPD and PPDM groups, while there was a gap between the bone tissue and the PEEK scaffold surface in the PP group. Bone-implant contact was consistently higher in the PPD and PPDM groups than in the PP group at all time points (Fig. 8F).

4. Discussion

4.1. Design and construction of surface-activated porous PEEK implants

PEEK materials are special engineering plastics with good mechanical properties, heat resistance and chemical resistance. PEEK products prepared by 3D printing can be used not only in aerospace and automotive manufacturing but also as an alternative to metal implants for clinical applications [31,32]. In this study, a 3D printer was specifically designed for PEEK material. Compared to conventional FDM printers, the molding bin temperature of the PEEK-specific printer can reach up to 250 $^{\circ}$ C, significantly reducing the gap between the print nozzle and the temperature of the molding bin, and the PEEK material can slowly crystallize under the high-temperature environment, releasing internal stress and effectively suppressing warpage and deformation. In addition, because PEEK prints are in a high-temperature environment for a long time during the printing process, the bond strength between the layers is continuously strengthened, the crystalline particles are continuously refined, and the crystallinity slowly increases, enabling the prints to have high overall strength and toughness. Mechanical tests showed that the elastic modulus of porous PEEK scaffolds was similar with cancellous bone. Although it was lower than solid PEEK, but the porous structure provided space for bone ingrowth and still has long-term advantages for implantation in vivo [33].

In the selection of surface modification methods for porous PEEK scaffolds, the simple but efficient surface modification method reported in the literature was preferred to reduce the complexity and ensure reproducibility, reliability, and safety to make it more promising for clinical translation. In recent years, PDA coatings have been widely used for the surface biofunctionalization of implant materials because of their simple preparation, good biocompatibility and strong adhesion [34]. In many surface modification studies of PEEK implants, PDA often serves as a bridge between the implant and bioactive molecules. Compared to solid PEEK implants, porous PEEK scaffolds have a larger specific surface area and therefore are theoretically able to fully exploit the surface modification benefits of PDA. Bioactive magnesium ions are known for their multifunction on promoting osteogenesis [35,36], angiogenesis [27], neurological function regulation [37] and anti-tumor [38,39], and they can be immobilized on the PDA coating through chelation. In this study, a combination of PDA and Mg²⁺ was used as the surface modification method for porous PEEK scaffolds (PPDM group). The hydrophilicity of the bone implant material is an important factor affecting the osseointegration capacity, and studies have shown that increased hydrophilicity of the material can promote the adhesion and differentiation of bone progenitor cells [40], enhance the amount of bone attachment on the implant surface [41], and accelerate the rate of mineralization deposition on the implant surface [42]. For porous implants, the enhanced hydrophilicity also facilitates the flow of internal body fluids and the recruitment and adhesion of cells. Since PDA is rich in hydrophilic groups such as carboxyl, amino, imino, and phenol groups, the hydrophilicity of porous PEEK scaffolds was significantly enhanced by PDA surface modification.

4.2. In vitro studies of angiogenesis and osteogenic differentiation

For bone repair materials, excellent biocompatibility means that the implants promote the development of tissues and cells in the bone defect environment, including proliferation and adhesion of osteogenic-associated cells, differentiation of bone progenitor cells, integration of bone tissue with the implant material, and osteogenesis-associated angiogenesis. In a stricter definition, the biological activity of a

biomaterial is limited to the region of the interface where the material binds to the host, which is called the "bioactive zone" [43]. In this study, to investigate the differences in the bioactive zone of porous PEEK scaffolds in each group, MC3T3-E1 cells and HUVECs were cocultured with different groups of porous PEEK scaffolds by direct contact and indirect contact, and cell proliferation, adhesion, osteogenic differentiation, migration, and angiogenesis were examined using different experimental methods.

First, the cytotoxicity of different groups of porous PEEK scaffolds was investigated. The biosafety of PDA surface modification has been widely reported. Hee K et al. demonstrated that PDA does not inhibit the proliferation rate or cellular activity of a variety of mammalian cell types, including fibroblasts, osteoblasts, endothelial cells, and neurons [44]. The application of PDA in vivo is also considered to be safe, and the LD50 of intravenous input of PDA nanoparticles determined by Liu Y et al. ranged from 400.22 to 585.19 mg/kg, indicating low acute toxicity [45]. Our experimental results indicate that magnesium ions and PDA surface modification do not inhibit cell proliferation or increase the rate of apoptosis. The release of magnesium ions from the PPDM group scaffolds promoted the proliferation of MC3T3-E1 cells and HUVECs, which also confirms the bioactive manifestations of magnesium ions reported in the literature [46]. Then, the effects of the scaffolds on cell adhesion were investigated. The interaction of cells with the material surface profoundly affects the biocompatibility of the implant and cell adhesion to the implant surface is essential to obtain an optimal host-implant response. This study verified that both PDA and Mg²⁺ could improve cell adhesion on the surface of PEEK materials. And Mg^{2+} could increase the expression of vinculin protein in MC3T3-E1 and HUVECs.

The effect of implants on cellular osteogenic differentiation is an important factor in determining the rate of bone regeneration. The nature of bone as a mineralized connective tissue depends on the function and interaction of the cells with the extracellular matrix. The functional role of osteoblasts in bone formation is divided into three main stages. The first stage is the adhesion and proliferation of osteoblasts, and previous experiments have demonstrated that porous PEEK scaffolds modified with bioactive coatings can promote the proliferation and adhesion of MC3T3-E1 osteogenic precursor cells; the second stage is osteogenic differentiation, which is the process of differentiation and maturation of osteoblasts from osteogenic precursor cells into osteoblasts. The third stage is extracellular matrix mineralization, in which mature osteoblasts form a bone matrix through calcium and phosphorus deposition [47,48]. In this study, the modified porous PEEK scaffold could promoted the expression of Runx2, Col1, Alp, and Opn genes and the expression of RUNX2, COL1, OPN, and Osterix proteins in MC3T3-E1 cells. RUNX2 and Osterix are specific transcription factors that regulate osteoblast matrix protein expression and are essential for osteogenic differentiation and bone formation [49]. COL1 is an important component of the bone matrix produced by osteoblasts and OPN is a more abundant noncollagenous protein in the bone matrix, both of which are important for osteoblast adhesion, differentiation and bone matrix formation [50]. In addition, no difference was found in the expression of the Bmp2 and Ocn genes between groups, likely because Mg2+ and PDA surface modification did not cause activation of BMP2, whereas OCN proteins tend to appear at the end of osteogenic differentiation [51] and therefore did not show differences in early gene expression.

ALP is a typical protein product produced during osteoblast proliferation and differentiation and extracellular matrix maturation; therefore, ALP activity is often used to indicate the early degree of osteoblast differentiation [52]. ALP staining results showed that Mg²⁺ and PDA were able to significantly shift the time point of cell differentiation maturation forward. The results of calcium nodules staining showed that the time point of extracellular matrix mineralization of MC3T3-E1 cells cocultured with porous PEEK scaffolds modified with Mg²⁺ and PDA bioactive coatings was also significantly shifted forward. The above experimental results indicate that the PDA surface modification

significantly enhances the ability of the porous PEEK scaffold interface to contribute to bone differentiation, and the presence of ${\rm Mg}^{2+}$ not only further enhances this effect but also promotes osteoblast differentiation around the porous PEEK scaffold.

Timely and adequate angiogenesis during bone defect repair is also crucial to the speed of bone repair. Neovascularization not only provides a large amount of oxygen and nutrients, but also a constant supply of bone progenitor cells and calcium and phosphorus ions for the formation of bone matrix and bone units. In this study, the effects of different groups of porous PEEK scaffolds on HUVECs were analyzed via scratch assay and tubule formation assays, and the results showed that the porous PEEK scaffolds modified with a ${\rm Mg}^{2+}$ and PDA coating enhanced the migration ability and tubule formation of HUVECs compared with unmodified and PDA modified porous PEEK scaffolds. Recent studies have shown that H-type vessels are able to regulate the spatial and temporal coupling of angiogenic and osteogenic processes. Within bone tissue, oxygen-rich blood flows out of arteries, first into H-type vessels with high CD31 and EMCN expression, then into L-type vessels at the epiphysis and epiphyseal junction, and finally into the central vein [53]. The effects of different groups of porous PEEK scaffolds on the expression of H-type vascular endothelial markers were investigated, and the expression levels of CD31 and EMCN were higher in the PPDM group than that in the PP and PPD groups, while there was no significant difference in protein expression between the PP and PPD groups. Therefore, it could be concluded that Mg²⁺ can upregulate the expression of H-type vascular markers in HUVECs in vitro, which is consistent with the results observed by Zhang D et al. in their experiments [54].

4.3. In vivo studies of osseointegration in an animal model

Although many studies have now reported the applications of PDAmediated surface modifications in porous metal or PEEK scaffolds, in vivo studies of the osteogenic and angiogenic effects of these surface modifications are not sufficiently advanced [55-58]. Therefore, to evaluate the osseointegration ability and bioactivity of porous PEEK scaffolds during in vivo bone defect repair, the scaffolds were implanted into the femoral condyles of rabbits and differences in internal vessel ingrowth and bone ingrowth in porous PEEK scaffolds in each group were analyzed at different time points after implantation. Micro-CT analysis of vascular ingrowth inside the porous PEEK scaffolds showed that vascular ingrowth was most pronounced at 4 weeks after implantation, and the PPDM group had a significantly higher vessel volume fraction and vessel diameter parameters than the PP and PPD groups at all time points. Combined with the magnesium ion release profile in the PPDM group scaffolds and the contributing vascular performance in vitro, it could be concluded that the PPDM group scaffolds were able to promote vessel growth inside the porous PEEK scaffolds by releasing magnesium ions early after implantation. The bone ingrowth in porous PEEK scaffolds was also analyzed by micro-CT. The bone volume fraction inside the scaffolds was higher in the PPD and PPDM groups than in the PP group at all time points, demonstrating the significant bone ingrowth and osseointegration advantages of the porous PEEK scaffolds after surface modification. Due to these results combined with the characteristics of vascular ingrowth inside the porous PEEK scaffolds, it was proposed that the angiogenic advantages of magnesium ions can accelerate bone ingrowth in the early stage after implantation.

Through hard tissue sectioning, the vascular morphology inside the porous PEEK scaffolds was directly observed microscopically, and the number and thickness variations of the vessels corroborate the results of micro-CT analysis. Bone ingrowth was also observed inside all the porous PEEK scaffolds, and even in porous PEEK scaffolds without surface modification, the fraction of bone volume observed inside the scaffolds in histological sections was close to 10% at week 12. Because histologic sections only showed differences in bone ingrowth in a single section of the porous PEEK scaffold, the differences in bone ingrowth between the scaffold groups were not significant compared with the

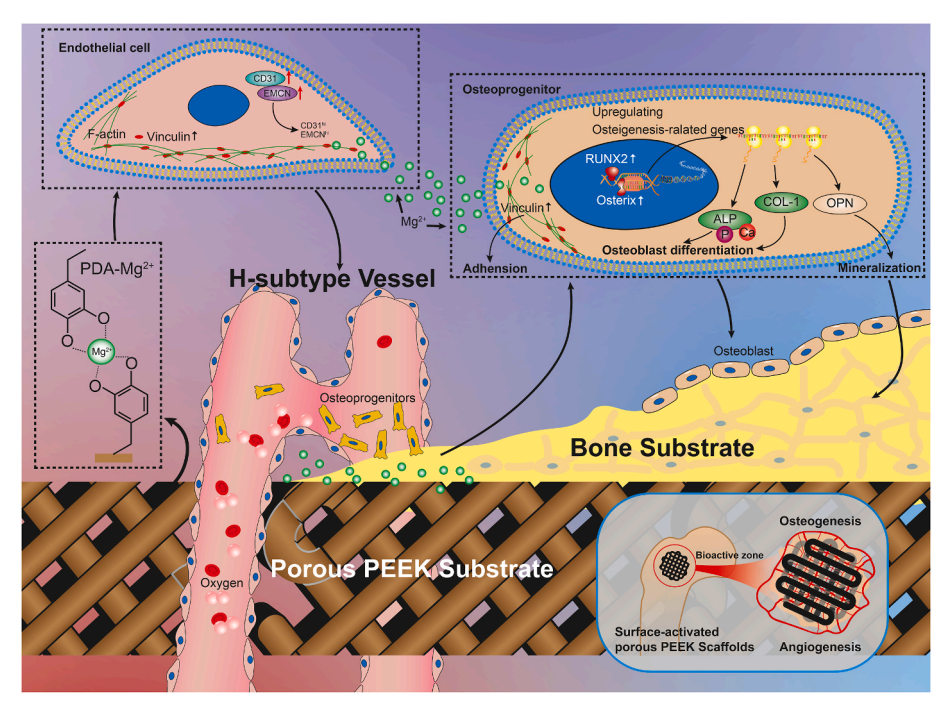


Fig. 9. The mechanism by which magnesium surface-activated 3D-printed porous PEEK scaffolds promote angiogenesis and osteogenesis.

results of the Micro-CT analysis. However, the contact ratio of new bone to the scaffold surface was significantly higher in the PPD and PPDM groups than the PP group, indicating that the PDA surface modification significantly enhanced the interfacial osseointegration ability of the porous PEEK scaffold.

Taken together, the *in vitro* and *in vivo* results verified that surface activation by ${\rm Mg}^{2+}$ and PDA is a promising approach to enhance the bioactivity and osseointegration ability of porous PEEK scaffolds. The angiogenesis and osteogenesis promoted by the scaffolds are shown in Fig. 9. Further studies will be performed to advance the evaluation of the long-term bone ingrowth effects and *in vivo* mechanical strength of porous PEEK scaffolds modified with magnesium-containing bioactive coatings to provide more convincing and valuable experimental data for clinical translation.

5. Conclusion

To address the characteristics and requirements of PEEK materials in bone defect applications, porous PEEK scaffolds with surface biofunctionalization were prepared using 3D printing technology, a PDA coating, and magnesium ion surface modification. Compared with unmodified porous PEEK scaffolds, porous PEEK scaffolds modified with magnesium-containing bioactive coatings showed an outstanding performance in vitro in terms of biological functions, such as promoting cell proliferation and adhesion, osteogenic differentiation, and vascularization. In vivo, the PDA coating significantly improved the poor interfacial osseointegration ability of porous PEEK scaffolds, while the release of magnesium ions enhanced bone ingrowth inside porous PEEK scaffolds by promoting early vascular ingrowth. This study significantly improved the osseointegration ability of PEEK materials through porous structure design and surface modification of PEEK materials, providing an improved method with high clinical translation potential for expanding the clinical applications of PEEK materials.

CRediT authorship contribution statement

Xinghui Wei: Conceptualization, Methodology, Formal analysis, Writing – original draft. **Wenhao Zhou:** Methodology, Investigation,

Writing – original draft. Zhen Tang: Methodology, Validation, Formal analysis. Hao Wu: Methodology, Validation. Yichao Liu: Formal analysis, Investigation, Visualization. Hui Dong: Resources, Investigation. Ning Wang: Formal analysis, Investigation. Hai Huang: Resources, Data curation. Shusen Bao: Formal analysis. Lei Shi: Investigation, Funding acquisition. Xiaokang Li: Conceptualization, Resources, Supervision. Yufeng Zheng: Writing – review & editing, Supervision. Zheng Guo: Conceptualization, Methodology, Supervision, Writing – review & editing.

Declaration of interests

The authors declare that they have no known competing financial interests or personal relationships that could have appeared to influence the work reported in this paper.

Acknowledgements

This work was supported by grants from the National Natural Science Foundation of China (No.51871239, No.32101087 and No.52171244).

Appendix A. Supplementary data

Supplementary data to this article can be found online at https://doi. org/10.1016/j.bioactmat.2022.05.011.

References

- [1] V. Campana, G. Milano, E. Pagano, et al., Bone substitutes in orthopaedic surgery: from basic science to clinical practice, J. Mater. Sci. Mater. Med. 25 (10) (2014) 2445–2461.
- [2] W. Wang, K.W.K. Yeung, Bone grafts and biomaterials substitutes for bone defect repair: a review, Bioact. Mater. 2 (4) (2017) 224–247.
- [3] M. Kaur, K. Singh, Review on titanium and titanium based alloys as biomaterials for orthopaedic applications, Mater. Sci. Eng. C 102 (2019) 844–862.
- [4] S. Kapoor, S.C. Kundu, Silk protein-based hydrogels: promising advanced materials for biomedical applications, Acta Biomater. 31 (2016) 17–32.
- [5] K. Lavanya, S.V. Chandran, K. Balagangadharan, et al., Temperature- and pHresponsive chitosan-based injectable hydrogels for bone tissue engineering, Mater. Sci. Eng. C 111 (2020), 110862.

- [6] E. Buck, H. Li, M. Cerruti, Surface modification strategies to improve the osseointegration of poly(etheretherketone) and its composites, Macromol. Biosci. 20 (2) (2020), e1900271.
- [7] M. Flejszar, P. Chmielarz, Surface modifications of poly(ether ether ketone) via polymerization methods-current status and future prospects, Materials 13 (4) (2020)
- [8] S.M. Kurtz, J.N. Devine, PEEK biomaterials in trauma, orthopedic, and spinal implants, Biomaterials 28 (32) (2007) 4845–4869.
- [9] M. He, Y. Huang, H. Xu, et al., Modification of polyetheretherketone implants: from enhancing bone integration to enabling multi-modal therapeutics, Acta Biomater. 129 (2021) 18–32.
- [10] C. Zhang, L. Wang, J. Kang, et al., Bionic design and verification of 3D printed PEEK costal cartilage prosthesis, J. Mech. Behav. Biomed. Mater. 103 (2020), 103641
- [11] D. Liu, J. Fu, H. Fan, et al., Application of 3D-printed PEEK scapula prosthesis in the treatment of scapular benign fibrous histiocytoma: a case report, J Bone Oncol 12 (2018) 78–82
- [12] V. Sgarminato, C. Tonda-Turo, G. Ciardelli, Reviewing recently developed technologies to direct cell activity through the control of pore size: from the macroto the nanoscale, J. Biomed. Mater. Res. B Appl. Biomater. 108 (4) (2020) 1176–1185
- [13] D.W. Hutmacher, Scaffolds in tissue engineering bone and cartilage, Biomaterials 21 (24) (2000) 2529–2543.
- [14] M.J. Lammi, J. Piltti, J. Prittinen, et al., Challenges in fabrication of tissue-engineered cartilage with correct cellular colonization and extracellular matrix assembly, Int. J. Mol. Sci. 19 (9) (2018).
- [15] P. Feng, P. Wu, C. Gao, et al., A multimaterial scaffold with tunable properties: toward bone tissue repair, Adv. Sci. 5 (6) (2018), 1700817.
- [16] H. Lee, S.M. Dellatore, W.M. Miller, et al., Mussel-inspired surface chemistry for multifunctional coatings, Science 318 (5849) (2007) 426–430.
- [17] Y. Liu, K. Ai, L. Lu, Polydopamine and its derivative materials: synthesis and promising applications in energy, environmental, and biomedical fields, Chem. Rev. 114 (9) (2014) 5057–5115.
- [18] A.P. Kusumbe, S.K. Ramasamy, R.H. Adams, Coupling of angiogenesis and osteogenesis by a specific vessel subtype in bone, Nature 507 (7492) (2014) 323-328
- [19] S. Stegen, N. Van Gastel, G. Carmeliet, Bringing new life to damaged bone: the importance of angiogenesis in bone repair and regeneration, Bone 70 (2015) 10, 27
- [20] U. Riaz, I. Shabib, W. Haider, The current trends of Mg alloys in biomedical applications-A review, J. Biomed. Mater. Res. B Appl. Biomater. 107 (6) (2019) 1970–1996.
- [21] M.P. Staiger, A.M. Pietak, J. Huadmai, et al., Magnesium and its alloys as orthopedic biomaterials: a review, Biomaterials 27 (9) (2006) 1728–1734.
- [22] D. Zhao, F. Witte, F. Lu, et al., Current status on clinical applications of magnesium-based orthopaedic implants: a review from clinical translational perspective, Biomaterials 112 (2017) 287–302.
- [23] P. Sikder, J.A. Ferreira, E.A. Fakhrabadi, et al., Bioactive amorphous magnesium phosphate-polyetheretherketone composite filaments for 3D printing, Dent. Mater. 36 (7) (2020) 865–883.
- [24] Y. Niu, L. Guo, F. Hu, et al., Macro-microporous surface with sulfonic acid groups and micro-nano structures of PEEK/nano magnesium silicate composite exhibiting antibacterial activity and inducing cell responses, Int. J. Nanomed. 15 (2020) 2403–2417.
- [25] T. Xiao, L. Fan, R. Liu, et al., Fabrication of dexamethasone-loaded dual-metalorganic frameworks on polyetheretherketone implants with bacteriostasis and angiogenesis properties for promoting bone regeneration, ACS Appl. Mater. Interfaces 13 (43) (2021) 50836–50850.
- [26] Y. Ren, P. Sikder, B. Lin, et al., Microwave assisted coating of bioactive amorphous magnesium phosphate (AMP) on polyetheretherketone (PEEK), Mater. Sci. Eng. C 85 (2018) 107–113.
- [27] Y. Lai, Y. Li, H. Cao, et al., Osteogenic magnesium incorporated into PLGA/TCP porous scaffold by 3D printing for repairing challenging bone defect, Biomaterials 197 (2019) 207–219.
- [28] Y. Li, S.K. Chen, L. Li, et al., Bone defect animal models for testing efficacy of bone substitute biomaterials, J Orthop Translat 3 (3) (2015) 95–104.
- [29] P. Gao, B. Fan, X. Yu, et al., In vitroBiofunctional magnesium coated Ti6Al4V scaffold enhances osteogenesis and angiogenesis and for orthopedic application, Bioact. Mater. 5 (3) (2020) 680–693.
- [30] P.K. Juan, F.Y. Fan, W.C. Lin, et al., Bioactivity and bone cell formation with polyε-caprolactone/bioceramic 3D porous scaffolds, Polymers 13 (16) (2021).
- [31] M. Rinaldi, F. Cecchini, L. Pigliaru, et al., Additive manufacturing of polyether ether ketone (PEEK) for space applications: a nanosat polymeric structure, Polymers 13 (1) (2021) 11.

- [32] S. a M. Tofail, E.P. Koumoulos, A. Bandyopadhyay, et al., Additive manufacturing: scientific and technological challenges, market uptake and opportunities, Mater. Today 21 (1) (2018) 22–37.
- [33] G. Lutzweiler, A. Ndreu Halili, N. Engin Vrana, The overview of porous, bioactive scaffolds as instructive biomaterials for tissue regeneration and their clinical translation, Pharmaceutics 12 (7) (2020).
- [34] W. Cheng, X. Zeng, H. Chen, et al., Versatile polydopamine platforms: synthesis and promising applications for surface modification and advanced nanomedicine, ACS Nano 13 (8) (2019) 8537–8565.
- [35] L. Ye, J. Xu, J. Mi, et al., Biodegradable magnesium combined with distraction osteogenesis synergistically stimulates bone tissue regeneration via CGRP-FAK-VEGF signaling axis, Biomaterials 275 (2021), 120984.
- [36] L.Z. Zheng, J.L. Wang, J.K. Xu, et al., Magnesium and vitamin C supplementation attenuates steroid-associated osteonecrosis in a rat model, Biomaterials 238 (2020), 119828.
- [37] Y. Zhang, J. Xu, Y.C. Ruan, et al., Implant-derived magnesium induces local neuronal production of CGRP to improve bone-fracture healing in rats, Nat. Med. 22 (10) (2016) 1160–1169.
- [38] J. Long, W. Zhang, Y. Chen, et al., Multifunctional magnesium incorporated scaffolds by 3D-Printing for comprehensive postsurgical management of osteosarcoma, Biomaterials 275 (2021), 120950.
- [39] X. Wei, Z. Tang, H. Wu, et al., Biofunctional magnesium-coated Ti6Al4V scaffolds promote autophagy-dependent apoptosis in osteosarcoma by activating the AMPK/ mTOR/ULK1 signaling pathway, Mater Today Bio 12 (2021), 100147.
- [40] L. Parisi, B. Ghezzi, M.G. Bianchi, et al., Titanium dental implants hydrophilicity promotes preferential serum fibronectin over albumin competitive adsorption modulating early cell response, Mater. Sci. Eng. C 117 (2020), 111307.
- [41] A. Wennerberg, R. Jimbo, S. Stübinger, et al., Nanostructures and hydrophilicity influence osseointegration: a biomechanical study in the rabbit tibia, Clin. Oral Implants Res. 25 (9) (2014) 1041–1050.
- [42] C. Vasak, D. Busenlechner, U.Y. Schwarze, et al., Early bone apposition to hydrophilic and hydrophobic titanium implant surfaces: a histologic and histomorphometric study in minipigs, Clin. Oral Implants Res. 25 (12) (2014) 1378–1385.
- [43] D.F. Williams, Biocompatibility pathways and mechanisms for bioactive materials: the bioactivity zone, Bioact. Mater. 10 (2022) 306–322.
- [44] S.H. Ku, J. Ryu, S.K. Hong, et al., General functionalization route for cell adhesion on non-wetting surfaces, Biomaterials 31 (9) (2010) 2535–2541.
- [45] Y. Liu, K. Ai, J. Liu, et al., Dopamine-melanin colloidal nanospheres: an efficient near-infrared photothermal therapeutic agent for in vivo cancer therapy, Adv. Mater. 25 (9) (2013) 1353–1359.
- [46] P. Gao, B. Fan, X. Yu, et al., In vitroBiofunctional magnesium coated Ti6Al4V scaffold enhances osteogenesis and angiogenesis and for orthopedic application, Bioact. Mater. 5 (3) (2020) 680–693.
- [47] J. Delgado-Calle, T. Bellido, The osteocyte as a signaling cell, Physiol. Rev. 102 (1) (2022) 379–410.
- [48] H. Fonseca, D. Moreira-Gonçalves, H.J. Coriolano, et al., Bone quality: the determinants of bone strength and fragility, Sports Med. 44 (1) (2014) 37–53.
- [49] F.M. Pérez-Campo, A. Santurtún, C. García-Ibarbia, et al., Osterix and RUNX2 are transcriptional regulators of sclerostin in human bone, Calcif. Tissue Int. 99 (3) (2016) 302–309.
- [50] R. Bou Assaf, K. Zibara, M. Fayyad-Kazan, et al., Healing of bone defects in pig's femur using mesenchymal cells originated from the sinus membrane with different scaffolds, Stem Cell. Int. (2019), 4185942, 2019.
- [51] Y. Han, X. You, W. Xing, et al., Paracrine and endocrine actions of bone-the functions of secretory proteins from osteoblasts, osteocytes, and osteoclasts, Bone Res 6 (2018) 16.
- [52] S. Sardiwal, P. Magnusson, D.J. Goldsmith, et al., Bone alkaline phosphatase in CKD-mineral bone disorder, Am. J. Kidney Dis. 62 (4) (2013) 810–822.
- [53] Y. Peng, S. Wu, Y. Li, et al., Type H blood vessels in bone modeling and remodeling. Theranostics 10 (1) (2020) 426–436.
- [54] D. Zhang, N. Ni, Y. Su, et al., Targeting local osteogenic and ancillary cells by mechanobiologically optimized magnesium scaffolds for orbital bone reconstruction in canines, ACS Appl. Mater. Interfaces 12 (25) (2020) 27889–27904.
- [55] L. Ma, S. Cheng, X. Ji, et al., Immobilizing magnesium ions on 3D printed porous tantalum scaffolds with polydopamine for improved vascularization and osteogenesis, Mater. Sci. Eng. C 117 (2020), 111303.
- [56] L. Deng, Y. Deng, K. Xie, AgNPs-decorated 3D printed PEEK implant for infection control and bone repair, Colloids Surf. B Biointerfaces 160 (2017) 483–492.
- [57] Y. Deng, X. Shi, Y. Chen, et al., Bacteria-triggered pH-responsive osteopotentiating coating on 3D-printed polyetheretherketone scaffolds for infective bone defect repair, Ind. Eng. Chem. Res. 59 (26) (2020) 12123–12135.
- [58] J. Wang, Y. Wang, Q. Wu, Poly(dopamine)-assisted bioactive coating on the surface of porous poly (ether ether ketone) to promote osteogenic differentiation of rBMSC, J. Wuhan Univ. Technol.-Materials Sci. Ed. 36 (5) (2022) 766–776.